

 Open access • Posted Content • DOI:10.1101/2020.07.31.231555

## **NAD modulates DNA methylation and cell differentiation** — [Source link](#)

[Simone Ummarino](#), [Simone Ummarino](#), [Mahmoud A. Bassal](#), [Yanzhou Zhang](#) ...+12 more authors

**Institutions:** [Harvard University](#), [Beth Israel Deaconess Medical Center](#), [University of Eastern Piedmont, University of Milan](#)

**Published on:** 02 Aug 2020 - [bioRxiv](#) (Cold Spring Harbor Laboratory)

**Topics:** [Epigenetic Profile](#), [Cellular differentiation](#), [Epigenome](#), [Epigenetics](#) and [DNA methylation](#)

Related papers:

- [NAD Modulates DNA Methylation and Cell Differentiation](#)
- [Epigenetics: Connecting Environment and Genotype to Phenotype and Disease](#)
- [Epigenetic control of reprogramming and cellular differentiation.](#)
- [Epigenetics: Reprogrammable interface of the genome and environments.](#)
- [Epigenetic Modulators of Monocytic Function: Implication for Steady State and Disease in the CNS](#)

Share this paper:    

View more about this paper here: <https://typeset.io/papers/nad-modulates-dna-methylation-and-cell-differentiation-1tsj1cmgl9>

Ummarino *et al.*

## **NAD modulates DNA methylation and cell differentiation.**

1  
2  
3  
4  
5  
6  
7  
8  
9  
10  
11  
12  
13  
14  
15  
16  
17  
18  
19  
20  
21  
22  
23  
24  
25  
26  
27  
28  
29  
30  
31  
32  
33  
34

Simone Ummarino<sup>1,2,3</sup>, Mahmoud A. Bassal<sup>1,2,3,4\*</sup>, Yanzhou Zhang<sup>1,2,3\*</sup>, Andy Joe Seelam<sup>5,6</sup>, Ikei S. Kobayashi<sup>3</sup>, Marta Borchiellini<sup>5</sup>, Alexander K. Ebralidze<sup>1,2,3</sup>, Bon Q. Trinh<sup>1,2,3</sup>, Susumu S. Kobayashi<sup>2,3,7</sup>, Annalisa Di Ruscio<sup>1,2,3,5</sup>

\*These two authors equally contributed to the work

1 Harvard Medical School Initiative for RNA Medicine, Harvard Medical School, Boston, MA, 02115, USA

2 Harvard Stem Cell Institute, Harvard Medical School, Boston, MA, 02115, USA

3 Department of Medicine, Beth Israel Deaconess Medical Center, Harvard Medical School, Boston, 02215, MA, USA

4 Cancer Science Institute, National University of Singapore, 117599, Singapore

5 University of Eastern Piedmont, Department of Translational Medicine, Novara, 28100, Italy

6 International Center for T1D, Pediatric Clinical Research Center “Romeo Ed Enrica Invernizzi”, Department of Biomedical and Clinical Science L. Sacco, Università Degli Studi Di Milano, Milan, Italy

7 Division of Translational Genomics, Exploratory Oncology Research & Clinical Trial Center, National Cancer Center, Kashiwa, 277-8577, Japan

Corresponding author  
Annalisa Di Ruscio  
Center for Life Science, Room 404  
3 Blackfan Circle,  
Boston, MA 02115  
Tel: 617-735-2022  
FAX: 617-735-2222  
adirusci@bidmc.harvard.edu

Ummarino *et al.*

## 35 **Abstract**

36 Nutritional intake impacts the human epigenome by directing epigenetic pathways in normal cell  
37 development via as yet unknown molecular mechanisms. Consequently, imbalance in the nutritional  
38 intake is able to dysregulate the epigenetic profile and drive cells towards malignant transformation.  
39 Herein, we present a novel epigenetic effect of the essential nutrient, NAD. We demonstrate that  
40 impairment of DNMT1 enzymatic activity by NAD-promoted ADP-ribosylation, leads to  
41 demethylation and transcriptional activation of *CEBPA* gene, suggesting the existence of an  
42 unknown NAD-controlled region within the locus. In addition to the molecular events, NAD treated  
43 cells exhibit significant morphological and phenotypical changes that correspond to myeloid  
44 differentiation.

45 Collectively, these results delineate a novel role for NAD in cell differentiation and indicate  
46 novel nutri-epigenetic strategy to regulate and control gene expression in human cells.

## 48 **Introduction**

49 Malnutrition and obesity are associated to epigenetic dysregulation thereby promoting cellular  
50 transformation and cancer initiation (Avgerinos, Spyrou et al., 2019, Birks, Peeters et al., 2012). A  
51 prolonged exposure to high-fat diet, poor nutrition and insults from environmental toxicants, all  
52 contribute to the epigenetic transgenerational inheritance of the obesity (King & Skinner, 2020).  
53 The degree of obesity, in term of body weight, is a well-documented risk factor for hematopoietic  
54 disease and cancer (Strom, Yamamura et al., 2009, Tedesco, Qualtieri et al., 2011). Together, these  
55 evidences highlight the importance of balanced micronutrient intake in order to preserve cell  
56 specific epigenetic programming and prevent anomalies that can potentially result in malignant  
57 transformation (Montgomery & Srinivasan, 2019, Yilmaz, Atilla et al., 2020).

58 In the last decade, numerous studies focusing on establishing a link between nutrition and  
59 epigenetics, led to the concept of “Precision Nutrition”; a translational approach based on the  
60 use of dietary compounds to direct epigenetic changes and drive normal cellular development

Ummarino *et al.*

61 (Zeisel, 2020). Natural compounds, like vitamins C and D, have been shown to slow pathological  
62 processes through their impact on the epigenome (Bunce, Brown et al., 1997, Nur, Rath et al.,  
63 2020). Similarly, nutri-epigenomic approaches have been shown to prevent several disease  
64 conditions including cancer (Di Tano, Raucci et al., 2020, Meroni, Longo et al., 2020).  
65 Nevertheless, the molecular mechanisms by which nutrients modulate the epigenome of healthy or  
66 cancer cells is largely unknown.

67 Nicotinamide adenine dinucleotide (NAD) is a dietary compound essential for life, and a  
68 coenzyme implicated in cellular redox reactions (Rajman, Chwalek et al., 2018). Maintenance of  
69 adequate levels of NAD is critical for cellular function and genomic stability (Ralto, Rhee et al.,  
70 2020). Few reports have shown that NAD precursors such as vitamin B3 (or nicotinic acid, NA) and  
71 nicotinamide (Nam) are able to drive cell differentiation in leukemic cell lines (Ida, Ogata et al.,  
72 2009, Iwata, Ogata et al., 2003), and impair cell growth. However, the molecular mechanism  
73 participating in these morphological changes remain unknown.

74 DNA methylation is a key epigenetic signature involved in transcriptional regulation, normal  
75 cellular development, and function (Jones, 2012). Methyl groups are added to the carbon 5 of  
76 cytosines in the context of CpG dinucleotides by specialized enzymes the DNA methyltransferase  
77 enzymes (DNMT1, 3A and 3B). While the bulk of the genome is methylated at 70–80% of its  
78 CpGs, CpG islands (CGI), that are clusters of CpG dinucleotides generally proximal to the  
79 transcription start sites (TSSs) of most human protein-coding genes, are mostly unmethylated in  
80 somatic cells. Numerous studies have established a link between aberrant promoter DNA  
81 methylation and gene silencing in diseases such as cancer (Herman & Baylin, 2003, Jones &  
82 Baylin, 2002).

83 NAD is also the substrate of Poly-(ADP) Ribose Polymerase 1 (PARP1) a nuclear protein that  
84 plays a pivotal role in gene regulation, and chromatin remodeling (Hageman & Stierum, 2001, Ray  
85 Chaudhuri & Nussenzweig, 2017). PARP1 utilizes NAD as a source of ADP-ribose moieties to  
86 assemble ADP-ribose polymers (PAR) and coordinate epigenetic modifications including DNA

Ummarino *et al.*

87 methylation (Ciccarone, Zampieri et al., 2017, Reale, Matteis et al., 2005). Several experimental  
88 data support a PARP1-mediated inhibition of DNA methyltransferase 1 (DNMT1) activity in  
89 human cell lines (Fang, Bi et al., 2015, Witcher & Emerson, 2009). These findings suggest a role  
90 for NAD in altering and, or facilitating modulation of DNA methylation, even if a direct link  
91 between demethylation and NAD treatment has not been established (Ciccarone, Valentini et al.,  
92 2014, Di Ruscio, Ebralidze et al., 2013).

93 Herein, we present a novel function of NAD, the ability to specifically demethylate and induce  
94 the expression of the hematopoietic master regulator, CCAAT/enhancer binding protein alpha  
95 (*CEBPA*) gene locus. The demethylation effect correlates with a total and local increase of ADP-  
96 ribose polymers (PAR) at the *CEBPA* promoter, thus supporting a NAD/PARP1/DNMT1 axis in  
97 which local inhibition of DNMT1, results in site-specific demethylation and transcriptional  
98 activation.

99 Our findings indicate NAD as a novel epigenetic modulator that counteracts the widespread  
100 epigenetic reprogramming concurring to obesity and cancers, and provide the first nutritional-based  
101 therapy for clinical interventions in these conditions.

102

## 103 **Materials and Methods**

### 104 *Cells and Cell Culture*

105 K562 cell line was purchased from ATCC and grown in RPMI medium supplemented with 10%  
106 fetal bovine serum (FBS), in the absence of antibiotics at 37°C, 5% CO<sub>2</sub>. The K562-*CEBPA*-ER  
107 line was grown in 12 well plate in phenol red-free RPMI 1640 (ThermoFisher Scientific, Cat. No.  
108 11835030), supplemented with 10% Charcoal stripped FBS (Sigma Aldrich, Cat. No. F6765), and 1  
109 µg/mL puromycin, beginning at a density of 0.2 x 10<sup>6</sup> cells/mL. 1µM estradiol (Sigma Aldrich,  
110 Cat. No. E2758) was added from a 5-mM stock solution in 100% ethanol to induce *CEBPA*-ER  
111 nuclear translocation and a corresponding amount of ethanol (0.02%) to mock-treated cells as

Ummarino *et al.*

112 controls. Viable cells excluding trypan blue were enumerated every day and used for the experiment  
113 (D'Alo, Johansen et al., 2003, Umek, Friedman et al., 1991).

114

115 *NAD treatment*

116 K562 cells were incubated with 0.1, 0.5, 1, 1.5 or 10 mM of NAD (Sigma Aldrich) or vehicle  
117 (milliQ water) for four days at 37°C. Cells were counted every day and cell pellets were collected to  
118 perform all the downstream analysis. *Colorimetric NAD assay*. The BioVision NAD/NADH  
119 Quantification Colorimetric Kit was used according to the manufacturer's instructions (BioVSION).  
120 Briefly, K562 cells were homogenized by two cycles of freezing and thawing in 400µl of BioVSION  
121 NAD/NADH extraction buffer. The homogenate was filtered using BioVision 10-kD cut-off filters  
122 (10000 g, 25 min, 4°C). To detect only NADH content, NAD was decomposed by heating 200µl of  
123 the homogenate. The homogenate of decomposed and non-decomposed samples was distributed in  
124 a 96 well plate, the developer solutions was added to the samples. The absorbance (OD 450nm) was  
125 acquired for 30 minutes using the VICTOR Multilabel Plate Reader (Perkin Elmer).

126

127 *K562 Wright Giemsa staining*

128 Approximately  $2 \times 10^4$  per each sample, were spotted on a slide using the cytopspin at 400 rpm for  
129 5 min. The cells were then stained with the Wright Giemsa solutions kit (CAMCO STAIN PAK,  
130 pc#702) according to manufacturer's instructions.

131

132 *Nitroblue Tetrazolium (NBT) assay*

133 Nitroblue blue tetrazolium (NBT) analysis was performed using  $5 \times 10^5$  cells incubated in a 1 mL  
134 solution containing phosphate-buffered saline (PBS), NBT (Sigma), and 0.33 µM phorbol myristate  
135 acetate (PMA) for 20 minutes at 37°C. The reaction was then stopped by incubation on ice. Cells  
136 were immediately fixed on slides by cytocentrifugation and counterstained with 0.5% safranin O in  
137 20% ethanol.

Ummarino *et al.*

138 *Immunofluorescence*

139 Cells were fixed with PFA 2% (Paraformaldehyde/MeOH), washed with 1X Phosphate-buffered  
140 saline (PBS), and permeabilized with 0.5 % Triton X100. After blocking with 7% Goat-serum, for  
141 30 min, cells were incubated with primary antibody Anti poly (ADP-ribose) polymer (1:400  
142 Abcam, ab 14459) overnight at 4°C, covered from the light. The following day, cells were washed  
143 with 1X PBS, and incubated with secondary antibody goat anti-mouse (1:500, Alexa Fluor 555) for  
144 1hr, re-washed, and nuclei counterstained with Prolong gold antifade mountant already containing  
145 DAPI (Thermo Fisher Scientific). Samples were analysed on a Leica DM 5500B Microscope with a  
146 100W high-pressure mercury lamp. Images were assembled and contrast-enhanced using Image J as  
147 per manufacturer's recommendations.

148

149 *RNA isolation and qRT-PCR analyses*

150 Total RNA isolation was carried out using TRIzol (Thermo-Fisher Scientific), as previously  
151 described (23). All RNA samples used in this study were treated with DNase I (10 U of DNase I per  
152 3 µg of total RNA; 37 °C for 1 hr; in the presence of RNase inhibitor). After DNase I treatment,  
153 RNA samples were extracted with acidic phenol (Sigma, pH 4.3) to eliminate any remaining traces  
154 of DNA. Taqman based qRT-PCR was performed using the one step Affymetrix HotStart-IT qRT-  
155 PCR Master Mix Kit (Affymetrix USB) and 50 ng of total RNA per reaction. Amplification  
156 conditions were 50°C (10 min), 95°C (2 min), followed by 40 cycles of 95°C (15s) and 60°C (1  
157 min). Target gene amplification was calculated using the formula  $2^{-\Delta\Delta C_t}$  as described (23), primer  
158 and probe sequences are listed in supplementary Tab 1.

159

160 *DNA isolation*

161 Cell pellets, resuspended in a homemade lysis buffer (0.5% SDS, 25 mM EDTA pH 8, 10 mM  
162 TRIS pH 8, 200 mM NaCl), were initially treated with RNase A (Roche) for 20 minutes at 37°C and  
163 then Proteinase K (Roche) overnight at 65°C. High quality genomic DNA was extracted by

Ummarino *et al.*

164 Phenol:chloroform:isoamyl Alcohol 25:24:1, pH:8 (Sigma) and precipitated with Isopropanol the  
165 following day. Genomic DNA was resuspended in Tris 1mM, EDTA 10mM (TE) pH 8 and stored  
166 at 4°C.

167

#### 168 *Western blotting analysis*

169 Whole-cell lysates from approximately  $2 \times 10^5$  cells per each sample were separated on 15%  
170 SDS-PAGE gels and transferred to a nitrocellulose membrane. Immunoblots were all blocked with  
171 5% nonfat dry milk in Tris-buffered saline, 0.1% (TBS-T) prior to incubation with primary  
172 antibodies. The Anti-poly (ADP-ribose) polymer (1:1000 Abcam, ab14459) was stained overnight  
173 at 4°C. For PARP1 and DNMT1 protein analyses, equivalent amount of whole-cell lysates were  
174 separated on 7 % SDS-PAGE gels and transferred to a nitrocellulose membrane. Immunoblots were  
175 stained overnight with the following primary antibodies: Anti-PARP1 (1:1000 Active motif,  
176 39559), Anti-DNMT1 (1:1000, Abcam, ab19905). All secondary horseradish peroxidase (HRP)-  
177 conjugated antibodies were diluted 1:5000 and incubated for 1hr at room temperature with TBST/  
178 5% milk. Immuno-reactive proteins were detected using the Pierce<sup>®</sup> ECL system (Thermo  
179 Scientific #32106).

180

#### 181 *Bisulfite Sequencing and Analysis*

182 DNA methylation profile of *CEBPA* locus was analyzed by bisulphite sequencing as previously  
183 described (Di Ruscio et al., 2013). Briefly, high molecular weight genomic DNA (1µg) was  
184 subjected to bisulfite conversion using the EZ DNA Methylation-Direct kit (Zymo Research)  
185 following the manufacturer's instructions. Polymerase chain reactions (PCR) on bisulfite converted  
186 DNA was performed with FastStart Taq DNA Polymerase (Roche) in the following conditions:  
187 95°C (6 min) followed by 35 cycles at 95°C (30 s) 53-57°C (1 min) 72°C (1 min), and a final step at  
188 72°C (7 min). Primers and PCR conditions for bisulfite sequencing are summarized  
189 in supplementary Tab 2. After gel purification, cloning into PGEM T-easy vector (Promega) and



Ummarino *et al.*

190 transformation in *E. coli* Competent Cells JM109 (Promega), 9 positive clones analyzed by Sanger  
191 sequencing for each sample. Only clones with a conversion efficiency of at least 99.6% were  
192 considered for further processed by QUMA: a quantification tool for methylation analysis  
193 (<http://quma.cdb.riken.jp/>) (Kumaki, Oda *et al.*, 2008).

194

#### 195 *Chromatin immunoprecipitation*

196 ChIP was performed as previously described (Zhang, Alberich-Jorda *et al.*, 2013). Briefly, K562  
197 cells were crosslinked with 1% formaldehyde (formaldehyde solution, freshly made: 50 mM  
198 HEPES-KOH; 100 mM NaCl; 1 mM EDTA; 0.5 mM EGTA; 11% formaldehyde) for 10 min at  
199 room temperature (RT) and 1/10<sup>th</sup> volume of 2.66 M Glycine was then added to stop the reaction.  
200 Cell pellets were washed twice with ice-cold 1X PBS (freshly supplemented with 1 mM PMSF).  
201 Pellets of 2 x10<sup>6</sup> cells were used for immunoprecipitation and lysed for 10 minutes on ice and  
202 chromatin fragmented using a Bioruptor Standard (30 cycles, 30 sec on, 60 sec off, high power).  
203 Each ChIP was performed with 10µg of antibody, incubated overnight at 4°C. A slurry of protein  
204 A or G magnetic beads (NEB) was used to capture enriched chromatin, which was then washed  
205 before reverse-crosslinking and proteinase K digestion at 65°C. Beads were then removed in the  
206 magnetic field and RNase treatment (5µg/µl Epicentre MRNA092) performed for 30 minutes at  
207 37°C. ChIP DNA was extracted with Phenol:chloroform:isoamyl Alcohol 25:24:1, pH:8 (Sigma)  
208 and then precipitated with equal volume of isopropanol in presence of glycogen. DNA pellet was  
209 dissolved in 30µl of TE buffer for following qPCR analyses. The following antibodies were used  
210 for ChIP: Anti-DNMT1 (Abcam, ab19905), Anti-poly (ADP-ribose) polymer (Abcam, ab14459),  
211 normal mouse IgG (Millipore 12-371b) and normal rabbit IgG (Cell Signaling 2729S). Fold  
212 enrichment was calculated using the formula  $2^{-\Delta\Delta Ct}$  (ChIP/non-immune serum). Primer sets  
213 used for ChIP are listed in supplementary Table 3.

214

215

Ummarino *et al.*

216 *Immunostaining for FACS analysis*

217 Anti-CD15-APC (Thermal Fisher Scientific, Cat. No. 17-0158-42), anti-CD14-FITC (Thermal  
218 Fisher Scientific, Cat. No. 11-0149-42) and anti-CD11b-Pacific blue (BioLegend, Cat. No. 101224)  
219 were incubated with  $1 \times 10^6$  K562 cells (vehicle or NAD treated) at 1:100 ratio. Cells were pre-  
220 incubated with anti-Fc receptor antibody (Thermal Fisher Scientific, Cat. No. 14-9161-73) at 1:20  
221 ratio to block Fc receptor before staining. Zombie red staining (BioLegend, Cat. No. 423109) was  
222 used as cell viability dye during FACS analysis. Cells were fixed using 2% PFA (Sigma, Cat. No.  
223 158127) before performing FACS analysis. Cell acquisition and analysis were performed on BD  
224 LSRFortessa (BD biosciences, CA, USA) using BD FACSDiva™ software (BD Bioscience).  
225 Analysis was performed using Flowjo software (Flowjo LLC, USA).

226

227 *Annexin V staining*

228 FITC Annexin V Apoptosis Detection Kit I (BD Bioscience) was used to determine the percentage  
229 of K562 undergoing apoptosis upon NAD treatment. All samples were prepared following the  
230 manufacturer's instructions. Briefly, cells were collected every day, washed twice with cold PBS and  
231 then resuspended in 1x Binding buffed at a concentration of  $1 \times 10^6$  cells/ml.  
232 Cells were incubated with 5µl fluorescein isothiocyanate (FITC) annexin V and 5µl Propidium Iodide  
233 for 15 min at room temperature in darkness. Analyses of cells viability and apoptosis were performed  
234 on BD LSR Fortessa (BD biosciences, CA, USA) using BD FACSDiva™ software (BD Bioscience).  
235 The data analysis was performed using Flowjo software (Flowjo LLC, USA).

236

237 *Seahorse analysis*

238 Mito Stress Test (Agilent Seahorse, 103015-100) assay was run as per manufacturers'  
239 recommendations. Briefly, on the day of assay, counted and PBS washed cells were suspended in  
240 XF Assay media (Agilent Seahorse Bioscience) pH adjusted to  $7.4 \pm 0.1$  supplemented with 4.5 g/L  
241 glucose (Sigma-Aldrich G7528), 0.11 g/L sodium pyruvate (Sigma-Aldrich) and 8 mM L-glutamine

Ummarino *et al.*

242 (Sigma-Aldrich).  $1 \times 10^5$  cells were added to each well of XFe24 Cell-Tak (Corning) pre-coated  
243 culture plates and then slowly centrifuged for incubation at 37°C in a non-CO<sub>2</sub> incubator. Oxygen  
244 consumption rate was measured at baseline using a Seahorse XFe24 according to standard protocols  
245 and after the addition of oligomycin (100 μM), carbonyl cyanide-4-(trifluoromethoxy)  
246 phenylhydrazone (FCCP, 100 μM) and rotenone and antimycin A (50 μM). Fold change was  
247 determined by normalizing raw values to the average of the second basal reading.

248

#### 249 *Statistical analysis*

250 All bisulfite sequenced clones were analyzed by Fisher's exact test. For mRNA qRT-PCR,  
251 *p*-values were calculated by t-test in GraphPad Prism Software. For both the analysis, values of *p*  
252 <0.05 were considered statistically significant (\**p* < 0.05; \*\**p* < 0.01; \*\*\**p* < 0.001). The Mean ±  
253 SD of duplicates is reported.

254

## 255 **Results**

256 *NAD inhibits cancer cell growth in a dose-dependent manner and drives accumulation of*  
257 *intracellular poly ADP-ribose polymers.*

258 NAD precursors drive myeloid differentiation and impair cell growth (Ida et al., 2009, Iwata et  
259 al., 2003). To examine whether similar effects could be mediated by NAD, K562 cells were  
260 cultured following a single addition of NAD or vehicle to the media, and tracked over four days  
261 (**Fig. 1a**). Cells were counted every day and cell pellets collected for downstream analyses (**Fig. 1a,**  
262 **b**). Inhibition of the cell growth, was observed across all the tested NAD concentrations in a dose-  
263 dependent manner, with the strongest effect at 10 mM, 96 hours upon treatment (**Fig. 1b**). Notably,  
264 this inhibition was not associated with apoptosis as demonstrated by the Annexin V staining,  
265 showing high viability (≈ 85%) of NAD-treated cells *versus* untreated (**Fig. S1a**). Consistently, the  
266 NAD/NADH content in the 10mM NAD treated cells, displayed nearly eightfold increase as  
267 compared to the baseline, already 24 hours after treatment (**Fig. 1c**). Provided that NAD is partially,

Ummarino *et al.*

268 utilized as a source of ADP-ribose units by PARP1 to build linear and branched poly ADP-ribose  
269 (PAR) polymers, NAD-treated and untreated K562 were stained with an anti-PAR antibody and  
270 examined by immunofluorescence to monitor the accumulation of PAR. Consistently, 24 hours  
271 upon NAD treatment, cells displayed an intense fluorescence signal in treated as compared to  
272 untreated cells, owing to the increased PAR synthesis and accumulation (**Fig. 1d**). These results  
273 mirrored the effects induced by 10-minutes treatment with hydrogen peroxide (H<sub>2</sub>O<sub>2</sub>), a known  
274 DNA damaging agent (Blenn, Althaus et al., 2006, Ryabokon, Cieslar-Pobuda et al., 2009, Valdor,  
275 Schreiber et al., 2008), associated with PAR production and therefore used as a positive control  
276 (**Fig. S1b**). Overall, these findings supported a PAR accumulation driven by NAD. As a further  
277 validation, PAR levels were analyzed by western blot. The strongest PAR band was detected on the  
278 first day and gradually decreased in the following days (**Fig. 1e**) likely due to PARs degradation by  
279 poly (ADP-ribose) glycohydrolases (PARGs) or similar pathway-related enzymes (O'Sullivan,  
280 Tedim Ferreira et al., 2019).

281 Collectively these data demonstrate that NAD inhibit cell growth and mediates accumulation of  
282 intracellular PAR as early as 24 hours upon treatment.

283

#### 284 *NAD treatment induces CEBPA distal promoter demethylation*

285 A PARP1-mediated inhibition of DNMT1 activity in human cell lines has been reported (Fang et  
286 al., 2015, Reale et al., 2005). Therefore, we reasoned that increase of NAD, a substrate of PARP1,  
287 could modulate genomic methylation. To this end, we investigated the methylation dynamics of the  
288 well-studied methylation-sensitive gene *CEBPA* in K562 cells, following treatment with 10mM  
289 NAD (Hackanson, Bennett et al., 2008, Zhang et al., 2013) *CEBPA* is a master transcription factor  
290 in the hematopoietic system, the loss or inhibition of which can result in block of differentiation and  
291 granulopoiesis, contributing to leukemic transformation. *CEBPA* promoter is aberrantly methylated  
292 in ~30% and ~51% of patients with chronic myeloid leukemia and acute myeloid leukemia,  
293 respectively (Hackanson et al., 2008, Iwata et al., 2003, Tenen, 2003). As *CEBPA* promoter,

Ummarino *et al.*

294 encompassing the -1.4 kb to -0.5 kb regions from the transcriptional start site (TSS), is methylated  
295 in K562, we decided to assess the impact of NAD treatment on DNA methylation profile. Using  
296 bisulfite sequencing, we surveyed three distinct regions located at -0.8 kb (-557; -857), -1.1kb (-  
297 895; -1.122), -1.4 kb (-1.120; -1.473) upstream to the TSS of *CEBPA* (**Fig. 2a**). NAD treatment led  
298 to concomitant decrease of DNA methylation levels within the distal promoter region (-0.8 kb  
299 (**Figs. 2b, c and S2a**) which equaled 44% reduction at 48 hours and dropped to 60%, 72 hours after  
300 NAD addition. These levels bounced back to a mild 17% decrease after 96 hours suggesting a  
301 dynamic re-establishment of DNA methylation levels within the site (**Fig. 2b, c**). In agreement with  
302 our earlier findings (**Fig. 1d,e**), wherein the strongest accumulation of PARs was observed 24 hours  
303 post-NAD treatment (**Fig. 1d,e**), these results seem to indicate that the additional 24 hours were  
304 required to inhibit DNMT1 enzymatic activity and promote the methylation changes observed over  
305 the 48 and 72 hour time points (**Fig. 2b,c**). Unexpectedly, only minor changes in the distal promoter  
306 I (-1.1kb) and II (-1.4kb) were detected at 72 hours, suggesting a certain specific modality of NAD-  
307 mediated demethylation (**Figs. 2d, e and S2a**). Consistent with previous reports, DNA methylation  
308 within the -1.1kb and -1.4kb regions, does not correlate with *CEBPA* expression in both K562 and  
309 AML samples using conventional hypomethylating drugs (Hackanson et al., 2008).

310 Taken together these data demonstrate that the NAD-induced *CEBPA* promoter demethylation  
311 relies on a PAR-dependent mechanism which impairs DNMT1 activity

312  
313 *NAD treatment enhances CEBPA mRNA transcription in K562 by a PARP1- dependent*  
314 *mechanism*

315 DNA methylation is a key epigenetic signature involved in gene regulation. To investigate  
316 whether NAD-induced demethylation of *CEBPA* distal promotor was associated with increased  
317 levels of *CEBPA* transcriptional activation, we measured the *CEBPA* expression by qRT PCR in  
318 cells treated with 10 mM NAD (**Fig. 3a**), over multiple time points. Upregulation of *CEBPA*, 72-  
319 and 96-hour- upon treatment was observed only in cells treated with the highest NAD concentration

Ummarino *et al.*

320 (**Figs. 3a and S2b**). These results parallel *CEBPA* upregulation at 72 and 96 hours following  
321 demethylation of the distal promoter using the standard hypomethylating agent 5-aza-2'-  
322 deoxycytidine in K562 cells (Hackanson et al., 2008). As the only region sensitive to NAD-induced  
323 demethylation effect corresponded to *CEBPA* distal promoter, while nearly no changes occurred in  
324 the two upstream regions (-1.4 kb and -1.1kb) we reasoned the involvement of epigenetic regulators  
325 to account for this site selectivity. Previous studies have reported that PARP1 assembled ADP-  
326 ribose polymers are able to impair DNMT1 activity in human and murine cell lines (Reale et al.,  
327 2005). In following these findings, we hypothesized a mechanism wherein the NAD-induced  
328 production of PAR would specifically inhibit DNMT1 activity at *CEBPA* distal promoter, without  
329 affecting the more upstream regions. To test this hypothesis, we firstly verified the levels of PARP1  
330 and DNMT1 were not influenced by NAD at both expression and protein levels (**Figs. 3b and S2c**).  
331 Secondly, we performed quantitative Chromatin Immunoprecipitation (ChIP) with anti-PAR and  
332 anti-DNMT1 antibodies, 24 hours upon NAD treatment (**Fig. 3c-e**), given the strongest increase of  
333 PAR polymers at that specific time point (**Fig. 1d, e**). As expected, the *CEBPA* distal promoter  
334 region exhibited over 1.6-fold enrichment of PAR polymers than the vehicle treated cells, unlike the  
335 distal promoter II (**Fig. 3d, e**) in which the polymers were absent. Interestingly, DNMT1  
336 distribution between the distal promoter and the regions more upstream was unchanged (**Fig. 3e**),  
337 suggesting the same accessibility of DNMT1 for both sites, and a potential impairment of the  
338 enzymatic activity at the distal promoter due to the presence of the PAR polymers.

339 Collectively, these results indicate a PARP1-dependent demethylating mechanism boosted by  
340 NAD levels and enabling inhibition of DNMT1 activity in selected loci.

341  
342 *NAD induces myeloid differentiation.*

343 As previously reported NAD-precursors such as NA and other niacin-related compounds induce  
344 differentiation in immortalized cell lines, such as K562 and HL60 (Ida et al., 2009, Iwata et al.,  
345 2003). These findings prompted us to assess morphological changes upon NAD treatment. Wright

Ummarino *et al.*

346 Giemsa staining of K562 treated with 10mM NAD or vehicle revealed striking morphological  
347 changes four days after treatment (**Fig. 4a**). Specifically, vehicle treated cells exhibited a  
348 homogeneous population of round-shaped cells, with round or oval cell nuclei, whereas NAD-  
349 treated cells were more heterogeneous, with a higher cytoplasm:nucleus ratio, eccentrically located  
350 reniform nuclei with dense regions of heterochromatin and numerous vacuoles resembling a  
351 monocytic-macrophagic morphology. Additionally, NAD treatment leads to increases in nitroblue  
352 tetrazolium (NBT)-positive cells and expression of CD11b and CD14 surface markers indicating  
353 that NAD promotes monocytic-macrophagic differentiation in K562, whilst the absence of CD15  
354 expression ruled out a shift toward the granulocytic lineage (**Fig. 4b, c**) (Federzoni, Humbert et al.,  
355 2014). Hence, despite the reactivation of *CEBPA* mRNA, which is a master regulator of  
356 granulocytic differentiation, the expected morphological changes were not detected in NAD treated  
357 cells, although we could confirm increased expression of both CD15 and CD11b and not CD14  
358 upon ectopic expression of CEBPA protein as already shown previously (Federzoni et al., 2014,  
359 Perrotti, Cesi et al., 2002) (**Fig. S3a**). These results are not surprisingly since the oncogenic fusion  
360 protein: BCR-ABL, that is constitutively expressed in K562, suppresses *CEBPA* translation thus  
361 leading to transcriptional suppression of the granulocyte colony-stimulating factor receptor G-CSF-  
362 R and other myeloid precursor cells critical for granulocytic differentiation (Perrotti et al., 2002).  
363 Along with these data, we confirmed the absence of *CEBPA* protein by western blot analysis on  
364 K562 NAD-treated cells (data not shown).

365

#### 366 *NAD treatment improves mitochondrial OXPHOS function*

367 NAD has been previously demonstrated to restore mitochondrial function in aged mice and  
368 increase the intracellular ratio of NAD<sup>+</sup>/NADH, a critical cellular balance required for the Sirtuin 1  
369 (SIRT1) mediated activation of mitochondrial biogenesis (Chalkiadaki & Guarente, 2015, Khan,  
370 Auranen et al., 2014). To further investigate the NAD contribution to the mitochondrial function of  
371 K562, the Mito Stress Test was performed using a Seahorse XFe24 (**Fig. 4d**). Basal oxygen

Ummarino *et al.*

372 consumption rate (OCR) is used as a surrogate measure of mitochondrial function since  
373 mitochondria utilize oxygen to generate mitochondrial ATP. Our results show that NAD-treated  
374 K562 cells displayed a marginal increase in maximal oxygen consumption in response to Carbonyl  
375 cyanide-4 (trifluoromethoxy) phenylhydrazone (FCCP) stress. This translated to a 1.3-fold  
376 improvement in normalized maximal reserve capacity after only four days of co-incubation with  
377 NAD. Albeit a marginal change in maximal reserve capacity post NAD-treatment was observed,  
378 these results still highlight the significance NAD treatment plays on improving mitochondrial health  
379 and perhaps contributing to the changes described. The entire profile of K562 NAD-treated does not  
380 depart drastically from K562 untreated, but the increment of ORC emerging after the injection of  
381 FCCP, indicate variations in respiration capacity of K562 NAD-treated *versus* untreated, subjected  
382 to the same mitochondrial stimuli.

383

#### 384 **Discussion**

385 This study explores the demethylation impact brought about by NAD treatment. On the example  
386 of the *CEBPA* gene locus, silenced by DNA methylation in the leukemia model used herein,  
387 we carried out a molecular and biological dissection of the potential mechanism implicated in  
388 NAD-induced demethylation. We demonstrate that impairment of DNMT1 enzymatic activity, as a  
389 result from NAD-promoted ADP-ribosylation, leads to loss of *CEBPA* promoter methylation and  
390 corresponding transcriptional activation of *CEBPA* mRNA thereby revealing an unknown NAD-  
391 controlled region within the *CEBPA* locus.

392 NAD is regarded as a potential antiaging molecule, the levels of which tend to decline over our  
393 lifetime, yet the molecular mechanisms linking low NAD levels to aging are only partially  
394 understood (Bonkowski & Sinclair, 2016, Lautrup, Sinclair et al., 2019). As a critical substrate of  
395 SIRT and PARP enzyme family members, that are involved in multiple epigenetic pathways such as  
396 acetylation, ADP-ribosylation and DNA methylation, fluctuations of NAD levels may alter  
397 chromatin remodeling (Bai, 2015, Chalkiadaki & Guarente, 2015). An additional epigenetic role for



Ummarino *et al.*

398 NAD, independently of its partnering enzymes, has also been hypothesized by few reports wherein  
399 age- or nutrition-related decline of NAD levels were associated with the acquisition of abnormal  
400 DNA methylation profiles at specific loci (Chang, Zhang et al., 2010, Kane & Sinclair, 2019). *In*  
401 *vitro* evidence have also shown that ADP-ribosyl polymer impair DNMT1 enzymatic activity  
402 (Reale et al., 2005) and an ADP-ribosylation transcriptional control for the *P16* and *TET1* genes has  
403 been demonstrated (Ciccarone et al., 2014, Witcher & Emerson, 2009). To date over 2300 proteins,  
404 including DNMT1, have been reported as ADP-ribosylated (<http://ADPriboDB.leunglab.org>) but  
405 how ADP-ribosylation preserves the unmethylated state of certain regulatory sequences, remains  
406 elusive (Vivelo, Wat et al., 2017). In every instance studied, we demonstrate that NAD treatment  
407 induces production of PAR polymers, site-specific demethylation of *CEBPA* distal promoter and  
408 results in transcriptional activation of *CEBPA* mRNA in K562 cells (**Figs. 2,3**). These results led to  
409 hypothesize a site-selective demethylation mechanism wherein the NAD-induced production of  
410 PAR polymers inhibits DNMT1 activity at *CEBPA* distal promoter by preventing DNMT1  
411 interaction with the CGI, as described in the depicted model (**Fig. 4e**). The co-occurrence of PARs  
412 and DNMT1 on the distal promoter, but not on the distal promoter II, suggests a PAR-mediated  
413 specific inhibition of DNMT1 and reveals a NAD-responsive element on *CEBPA* promoter (**Fig. 3**).  
414 Intriguingly, the morphological changes along with the pronounced NBT staining and the positive  
415 shift of CD11b and CD14 surface markers, in addition to the improved mitochondrial function,  
416 seems to point to a monocytic-macrophagic-like transcriptional activation program initiated by  
417 NAD treatment (**Fig. 4**).

418 In conclusion, this study bridges a nutritional intervention to a molecular observation: increase of  
419 NAD levels in a cancer cell line results in local correction of DNA methylation. These data,  
420 therefore, provides a nutritional-guided approach for the prevention and the clinical management of  
421 cancers or other conditions associated with alteration of DNA methylation, potentially linked to  
422 decreased NAD levels.

423

Ummarino *et al.*

424 **Acknowledgements**

425 This work was supported by the National Institution of Health R00 CA188595, the Italian  
426 Association for Cancer Research (AIRC) Start-up Grant N.15347, the Giovanni Armenise-Harvard  
427 Foundation Career Development Award to ADR; the National Institution of Health (R01CA169259  
428 and R01CA240257) and Harvard Stem Cell Institute Blood Program (DP-0110-12-00) to SSK; the  
429 NCI K01CA222707 was awarded to BQT.

430

431 **Author contributions**

432 ADR supervised the project. ADR and SU conceived and designed the study and wrote the  
433 manuscript; SU, MAB, YZ, AJ, ISK, MB, SSK, performed experiments; BQT, MAB, SSK and  
434 AKE provided valuable suggestions about the project, and BQT, MAB, SSK critically reviewed the  
435 manuscript.

436

437 **Conflict of Interest**

438 SSK reports research grants and honorarium from Boehringer Ingelheim, grants from Taiho  
439 Pharmaceutical and MiNA therapeutics, and honorarium from Pfizer, Ono, Chugai, Astra Zeneca,  
440 and Roche outside the submitted work.

441 The other authors declare no conflict of interests.

442

443 **Data and materials availability:** All data and materials are available in the main text or the  
444 supplementary materials.

445

446 **References**

447 Avgerinos KI, Spyrou N, Mantzoros CS, Dalamaga M (2019) Obesity and cancer risk: Emerging  
448 biological mechanisms and perspectives. *Metabolism* 92: 121-135  
449 Bai P (2015) Biology of Poly(ADP-Ribose) Polymerases: The Factotums of Cell Maintenance. *Mol*  
450 *Cell* 58: 947-58

Ummarino *et al.*

- 451 Birks S, Peeters A, Backholer K, O'Brien P, Brown W (2012) A systematic review of the impact of  
452 weight loss on cancer incidence and mortality. *Obes Rev* 13: 868-91
- 453 Blenn C, Althaus FR, Malanga M (2006) Poly(ADP-ribose) glycohydrolase silencing protects  
454 against H<sub>2</sub>O<sub>2</sub>-induced cell death. *Biochem J* 396: 419-29
- 455 Bonkowski MS, Sinclair DA (2016) Slowing ageing by design: the rise of NAD(+) and sirtuin-  
456 activating compounds. *Nat Rev Mol Cell Biol* 17: 679-690
- 457 Bunce CM, Brown G, Hewison M (1997) Vitamin D and hematopoiesis. *Trends Endocrinol Metab*  
458 8: 245-51
- 459 Chalkiadaki A, Guarente L (2015) The multifaceted functions of sirtuins in cancer. *Nat Rev Cancer*  
460 15: 608-24
- 461 Chang J, Zhang B, Heath H, Galjart N, Wang X, Milbrandt J (2010) Nicotinamide adenine  
462 dinucleotide (NAD)-regulated DNA methylation alters CCCTC-binding factor (CTCF)/cohesin  
463 binding and transcription at the BDNF locus. *Proc Natl Acad Sci U S A* 107: 21836-41
- 464 Ciccarone F, Valentini E, Bacalini MG, Zampieri M, Calabrese R, Guastafierro T, Mariano G,  
465 Reale A, Franceschi C, Caiafa P (2014) Poly(ADP-ribosylation) is involved in the epigenetic  
466 control of TET1 gene transcription. *Oncotarget* 5: 10356-67
- 467 Ciccarone F, Zampieri M, Caiafa P (2017) PARP1 orchestrates epigenetic events setting up  
468 chromatin domains. *Semin Cell Dev Biol* 63: 123-134
- 469 D'Alo F, Johansen LM, Nelson EA, Radomska HS, Evans EK, Zhang P, Nerlov C, Tenen DG  
470 (2003) The amino terminal and E2F interaction domains are critical for C/EBP alpha-mediated  
471 induction of granulopoietic development of hematopoietic cells. *Blood* 102: 3163-71
- 472 Di Ruscio A, Ebralidze AK, Benoukraf T, Amabile G, Goff LA, Terragni J, Figueroa ME, De  
473 Figueiredo Pontes LL, Alberich-Jorda M, Zhang P, Wu M, D'Alo F, Melnick A, Leone G, Ebralidze  
474 KK, Pradhan S, Rinn JL, Tenen DG (2013) DNMT1-interacting RNAs block gene-specific DNA  
475 methylation. *Nature* 503: 371-6
- 476 Di Tano M, Raucci F, Vernieri C, Caffa I, Buono R, Fanti M, Brandhorst S, Curigliano G, Nencioni  
477 A, de Braud F, Longo VD (2020) Synergistic effect of fasting-mimicking diet and vitamin C against  
478 KRAS mutated cancers. *Nat Commun* 11: 2332
- 479 Fang YY, Bi FF, Zhou YM, Sun WP, Li CY, Liu Q, Zhao Y, Li D (2015) Nicotinamide adenine  
480 dinucleotide (NAD) may affect DNA methyltransferase 1 through regulation of BRCA1 in ovarian  
481 cancer. *Am J Cancer Res* 5: 1199-206
- 482 Federzoni EA, Humbert M, Torbett BE, Behre G, Fey MF, Tschan MP (2014) CEBPA-dependent  
483 HK3 and KLF5 expression in primary AML and during AML differentiation. *Sci Rep* 4: 4261
- 484 Hackanson B, Bennett KL, Brena RM, Jiang J, Claus R, Chen SS, Blagitko-Dorfs N, Maharry K,  
485 Whitman SP, Schmittgen TD, Lubbert M, Marcucci G, Bloomfield CD, Plass C (2008) Epigenetic  
486 modification of CCAAT/enhancer binding protein alpha expression in acute myeloid leukemia.  
487 *Cancer Res* 68: 3142-51
- 488 Hageman GJ, Stierum RH (2001) Niacin, poly(ADP-ribose) polymerase-1 and genomic stability.  
489 *Mutat Res* 475: 45-56
- 490 Herman JG, Baylin SB (2003) Gene silencing in cancer in association with promoter  
491 hypermethylation. *N Engl J Med* 349(21): 2042-2054
- 492 Ida C, Ogata S, Okumura K, Taguchi H (2009) Induction of differentiation in k562 cell line by  
493 nicotinic acid-related compounds. *Biosci Biotechnol Biochem* 73: 79-84
- 494 Iwata K, Ogata S, Okumura K, Taguchi H (2003) Induction of differentiation in human  
495 promyelocytic leukemia HL-60 cell line by niacin-related compounds. *Biosci Biotechnol Biochem*  
496 67: 1132-5
- 497 Jones PA (2012) Functions of DNA methylation: islands, start sites, gene bodies and beyond. *Nat*  
498 *Rev Genet* 13: 484-92
- 499 Jones PA, Baylin SB (2002) The fundamental role of epigenetic events in cancer. *Nature Reviews*  
500 *Genetics* 3: 415-428

Ummarino *et al.*

- 501 Kane AE, Sinclair DA (2019) Epigenetic changes during aging and their reprogramming potential.  
502 *Crit Rev Biochem Mol Biol* 54: 61-83
- 503 Khan NA, Auranen M, Paetau I, Pirinen E, Euro L, Forsstrom S, Pasila L, Velagapudi V, Carroll  
504 CJ, Auwerx J, Suomalainen A (2014) Effective treatment of mitochondrial myopathy by  
505 nicotinamide riboside, a vitamin B3. *EMBO Mol Med* 6: 721-31
- 506 King SE, Skinner MK (2020) Epigenetic Transgenerational Inheritance of Obesity Susceptibility.  
507 *Trends Endocrinol Metab* 31: 478-494
- 508 Kumaki Y, Oda M, Okano M (2008) QUMA: quantification tool for methylation analysis. *Nucleic  
509 Acids Res* 36: W170-5
- 510 Lautrup S, Sinclair DA, Mattson MP, Fang EF (2019) NAD(+) in Brain Aging and  
511 Neurodegenerative Disorders. *Cell Metab* 30: 630-655
- 512 Meroni M, Longo M, Rustichelli A, Dongiovanni P (2020) Nutrition and Genetics in NAFLD: The  
513 Perfect Binomium. *Int J Mol Sci* 21
- 514 Montgomery M, Srinivasan A (2019) Epigenetic Gene Regulation by Dietary Compounds in  
515 Cancer Prevention. *Adv Nutr* 10: 1012-1028
- 516 Nur SM, Rath S, Ahmad V, Ahmad A, Ateeq B, Khan MI (2020) Nutritive vitamins as epidrugs.  
517 *Crit Rev Food Sci Nutr*: 1-13
- 518 O'Sullivan J, Tedim Ferreira M, Gagne JP, Sharma AK, Hendzel MJ, Masson JY, Poirier GG  
519 (2019) Emerging roles of eraser enzymes in the dynamic control of protein ADP-ribosylation. *Nat  
520 Commun* 10: 1182
- 521 Perrotti D, Cesi V, Trotta R, Guerzoni C, Santilli G, Campbell K, Iervolino A, Condorelli F,  
522 Gambacorti-Passerini C, Caligiuri MA, Calabretta B (2002) BCR-ABL suppresses C/EBPalpha  
523 expression through inhibitory action of hnRNP E2. *Nat Genet* 30: 48-58
- 524 Rajman L, Chwalek K, Sinclair DA (2018) Therapeutic Potential of NAD-Boosting Molecules: The  
525 In Vivo Evidence. *Cell Metab* 27: 529-547
- 526 Ralto KM, Rhee EP, Parikh SM (2020) NAD(+) homeostasis in renal health and disease. *Nat Rev  
527 Nephrol* 16: 99-111
- 528 Ray Chaudhuri A, Nussenzweig A (2017) The multifaceted roles of PARP1 in DNA repair and  
529 chromatin remodelling. *Nat Rev Mol Cell Biol* 18: 610-621
- 530 Reale A, Matteis GD, Galleazzi G, Zampieri M, Caiafa P (2005) Modulation of DNMT1 activity by  
531 ADP-ribose polymers. *Oncogene* 24: 13-9
- 532 Ryabokon NI, Cieslar-Pobuda A, Rzeszowska-Wolny J (2009) Inhibition of poly(ADP-ribose)  
533 polymerase activity affects its subcellular localization and DNA strand break rejoining. *Acta  
534 Biochim Pol* 56: 243-8
- 535 Strom SS, Yamamura Y, Kantarijian HM, Cortes-Franco JE (2009) Obesity, weight gain, and risk  
536 of chronic myeloid leukemia. *Cancer Epidemiol Biomarkers Prev* 18: 1501-6
- 537 Tedesco J, Quattieri J, Head D, Savani BN, Reddy N (2011) High Prevalence of Obesity in Acute  
538 Promyelocytic Leukemia (APL): Implications for Differentiating Agents in APL and Metabolic  
539 Syndrome. *Ther Adv Hematol* 2: 141-5
- 540 Tenen DG (2003) Disruption of differentiation in human cancer: AML shows the way. *Nat Rev  
541 Cancer* 3: 89-101
- 542 Umek RM, Friedman AD, McKnight SL (1991) CCAAT-enhancer binding protein: a component of  
543 a differentiation switch. *Science* 251: 288-92
- 544 Valdor R, Schreiber V, Saenz L, Martinez T, Munoz-Suano A, Dominguez-Villar M, Ramirez P,  
545 Parrilla P, Aguado E, Garcia-Cozar F, Yelamos J (2008) Regulation of NFAT by poly(ADP-ribose)  
546 polymerase activity in T cells. *Mol Immunol* 45: 1863-71
- 547 Vivello CA, Wat R, Agrawal C, Tee HY, Leung AKL (2017) ADPriboDB: The database of ADP-  
548 ribosylated proteins. *Nucleic Acids Res* 45: 6254
- 549 Witcher M, Emerson BM (2009) Epigenetic silencing of the p16(INK4a) tumor suppressor is  
550 associated with loss of CTCF binding and a chromatin boundary. *Mol Cell* 34: 271-84

Ummarino *et al.*

551 Yilmaz M, Atilla FD, Sahin F, Saydam G (2020) The effect of malnutrition on mortality in  
552 hospitalized patients with hematologic malignancy. *Support Care Cancer* 28: 1441-1448  
553 Zeisel SH (2020) Precision (Personalized) Nutrition: Understanding Metabolic Heterogeneity. *Annu*  
554 *Rev Food Sci Technol* 11: 71-92  
555 Zhang H, Alberich-Jorda M, Amabile G, Yang H, Staber PB, Di Ruscio A, Welner RS, Ebralidze  
556 A, Zhang J, Levantini E, Lefebvre V, Valk PJ, Delwel R, Hoogenkamp M, Nerlov C, Cammenga J,  
557 Saez B, Scadden DT, Bonifer C, Ye M et al. (2013) Sox4 is a key oncogenic target in C/EBPalpha  
558 mutant acute myeloid leukemia. *Cancer Cell* 24: 575-88

559  
560

## 561 **FIGURE LEGENDS**

562 **Figure 1. NAD inhibits cancer cell growth in a dose-dependent manner and drives**  
563 **accumulation of intracellular poly ADP-ribose polymers.**

564 (A) Schematic of the experiment. K562 cells were cultured at different concentration of NAD:0.1,  
565 0.5, 1, 1.5, 10 mM or vehicle. Cell pellets, RNA and DNA samples were collected at different time  
566 point, 24, 48, 72, 96 hrs. (B) K562 growth curves in presence of NAD or vehicle. Cells were  
567 counted every 24 hrs for four days (C) The NAD/NADH content measured by colorimetric assay.  
568 The absorbance was measured at 450 nm every 24 hrs from the addition of NAD (10mM) to the cell  
569 culture media. NAD ratio was calculated according to the manufacturer's instructions (BioVision).  
570 (D) Immunofluorescence of PARs in K562 supplemented with of NAD (10mM) or vehicle after 24  
571 hrs. (E) PAR and PARP1 protein levels in K562 cells treated with NAD. The immunoblot band  
572 densities is measured using ImageJ and normalized by  $\beta$ -Actin.

573

574 **Figure 2. DNA methylation patterns of CEBPA upon NAD (10mM) or vehicle treatment.**

575 (A) Schematic representation of *CEBPA* locus. The three regions analysed in the promoter of  
576 *CEBPA* located at -0.8 kb (-557; -857), -1.1 kb (-895; -1.122) or -1.4 kb (-1.120; -1.473) from the  
577 TSS (+1) of the gene. (B, C) The methylation status of the distal promoter (the -0.8 kb region) was  
578 analysed at the three indicated time points. 9 clones were analysed, and lollipop graphs were  
579 generated using QUMA software. CpG methylation ratio consisting in methylated CpGs divided by  
580 unmethylated CpGs, was calculated by QUMA software. (D, E) Methylation status of distal  
581 promoter I (-1.1 kb) and distal promoter II (-1.4 kb) analysed 72hrs upon NAD (10mM) addition.

Ummarino *et al.*

582 Lollipop graphs were generated as described. (n=9 clones). All bisulfite sequenced clones were  
583 analysed by Fisher's exact test, \*:p<0.05; \*\*:p<0.01; \*\*\*:p<0.001

584

585 **Figure 3. NAD treatment enhances *CEBPA* transcription in K562 by a PARP1-dependent**  
586 **mechanism.** Panel (A) shows *CEBPA* mRNA levels upon 4 days treatment with NAD. The graph  
587 represents the average of two independent experiments (n=2). Panel (B) shows *PARP1* and *DNMT1*  
588 mRNA levels upon 4 days treatment with NAD. Chromatin was collected to perform ChIP assays  
589 with antibodies to PAR, DNMT1 and IgG (C-E). (C) Schematic of the *CEBPA* promoter regions  
590 screened by ChIP-qPCR analysis respectively at -1.4 kb and -0.8 kb from the TSS (double-headed  
591 arrows). (D) ChIP using PAR antibody and qPCR analysis of regions -1.4 kb (left panel) and -0.8  
592 kb (right panel). (E) ChIP using DNMT1 antibody and qPCR analysis of regions -1.4 kb (left panel)  
593 and -0.8 kb (right panel). Error bars indicate  $\pm$  S.D. \*:p<0.05; \*\*:p<0.01; \*\*\*:p<0.001

594

595 **Figure 4. NAD induces myeloid differentiation in K562.**

596 (A) Wright Giemsa staining showing morphological changes between NAD-treated and control  
597 cells after four days. (B) Increase in the surface markers CD15, CD14 and CD11b upon NAD  
598 treatment (C) NBT positive staining detected by small blue dots after counterstaining the cells with  
599 safranin. A magnification is shown in the rectangle. (D) Seahorse XF analysis of K562  
600 mitochondrial stress response in cells treated with NAD or vehicle. The figure represents the mean  
601 of two biological replicates (n=2). Error bars indicate  $\pm$  S.D. (E) Model showing the molecular  
602 mechanism of *CEBPA* gene reactivation by NAD. *CEBPA* is epigenetically silenced in K562.  
603 DNMT1 ensure a constant methylated status of *CEBPA* promoter (upper part). The NAD  
604 supplementation to K562 cell culture, boosts PARP1 to produce ADP-ribose polymers leading to  
605 DNMT1 inhibition (bottom part). The ultimate effect is *CEBPA* re-activated transcription.

606

Ummarino *et al.*

607 **Supplementary figure 1.** Cell viability upon NAD treatment. (A) K562 cells viability and  
608 apoptosis analyses upon NAD or vehicle (water) treatment. (B) Immunofluorescence analysis of  
609 PARs formation induced by 10 min-treatment with H<sub>2</sub>O<sub>2</sub> (100μM) in K562.

610

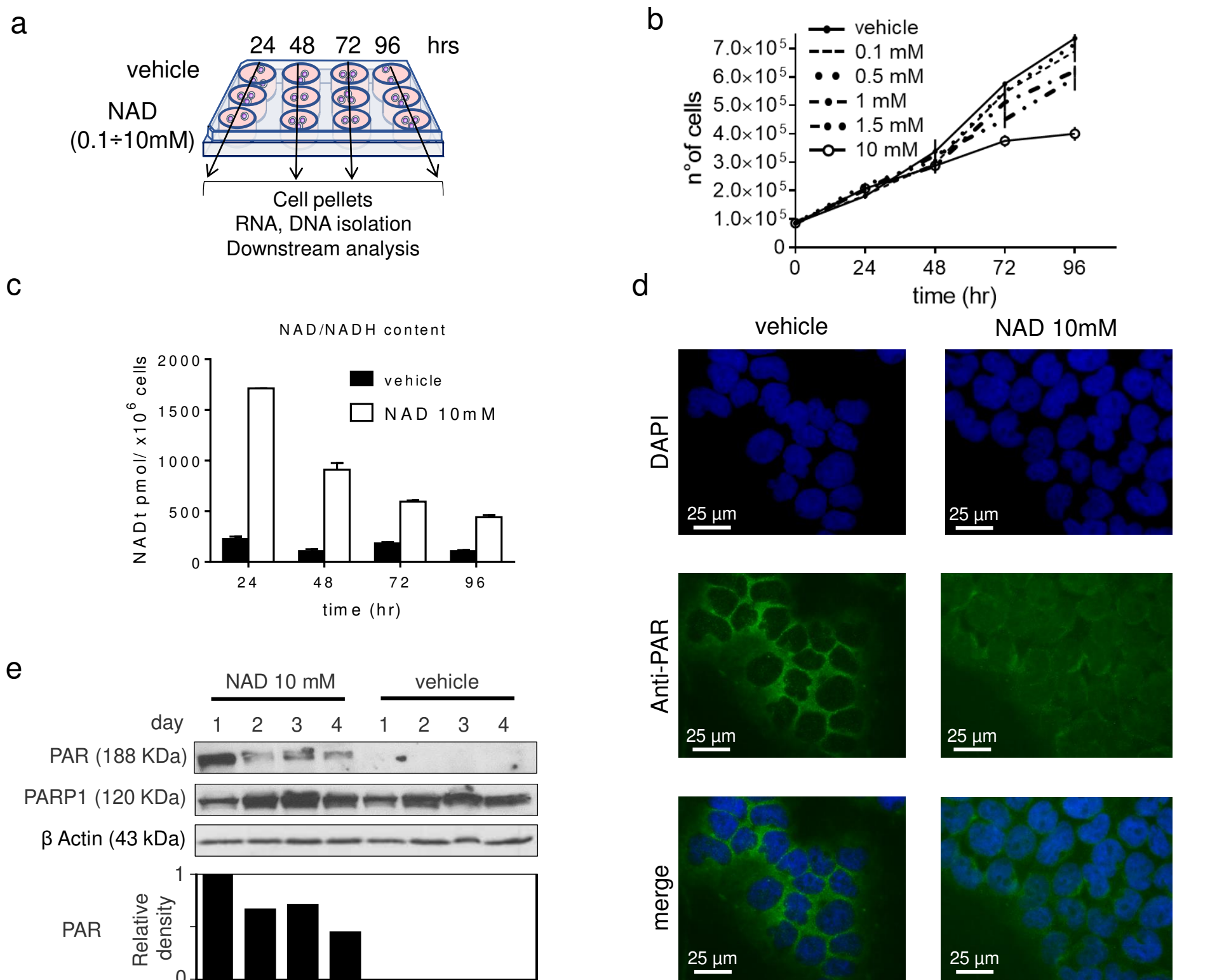
611 **Supplementary figure 2.** DNA methylation patterns and expression profile of *CEBPA* upon NAD  
612 or vehicle treatment. (A) Histograms representing the percentages of methylated CpGs (% Me  
613 CpGs) across *CEBPA* promoter 72hrs or 96hrs after treatment with NAD (10mM), calculated by  
614 Quma software. (B) expression levels of *CEBPA* in K562 treated for four days with either vehicle  
615 (water) or different concentration of NAD (0.1, 0.5, 1, 1.5 mM). (C) PARP1 and DNMT1 protein  
616 levels in K562 upon NAD treatment were monitored by western blot analysis.

617

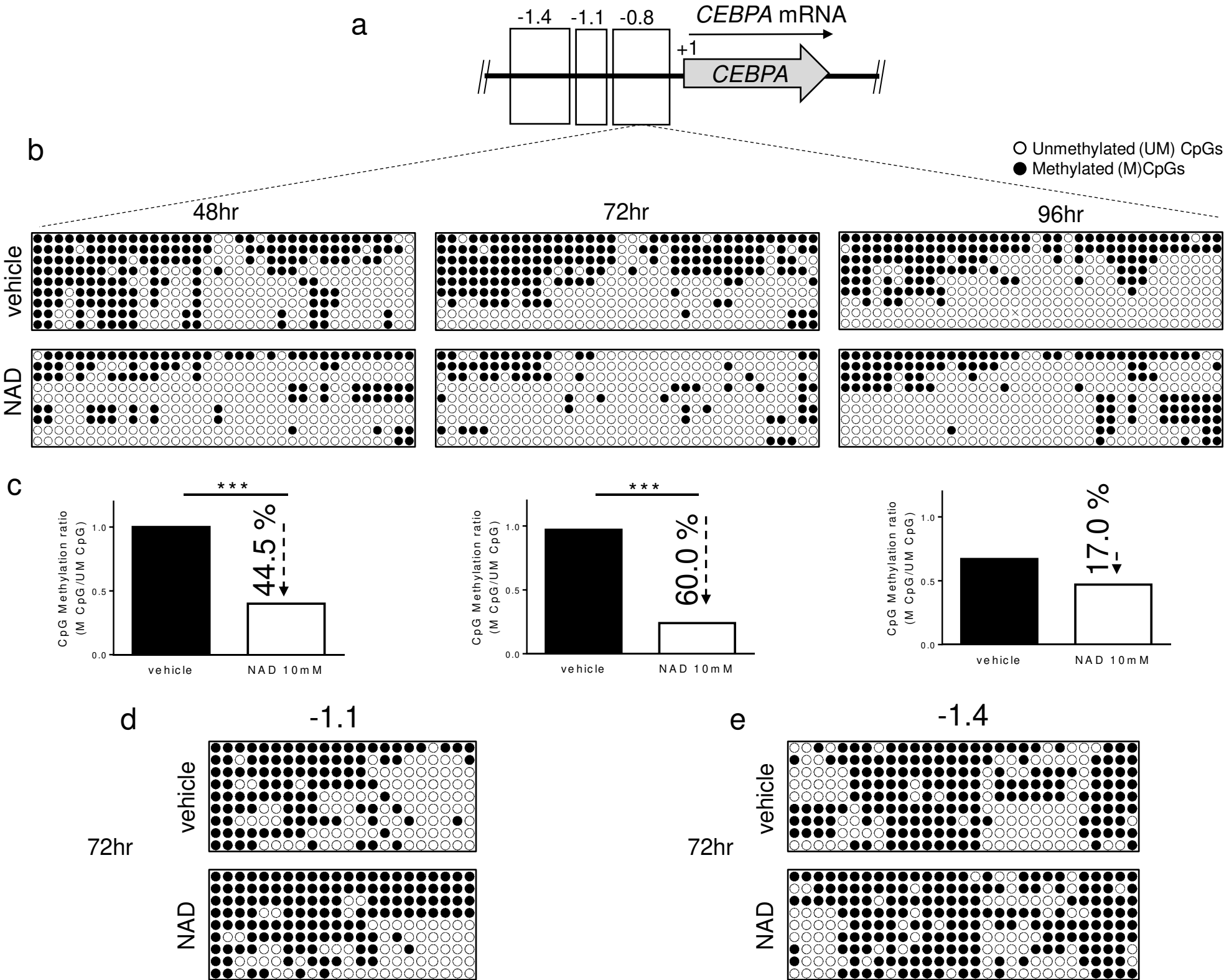
618 **Supplementary figure 3.** Flow cytometry analysis of CD14, CD15 and CD11b expression, in  
619 K562 wild type and K562-*CEBPA*-ER differentiated cells.

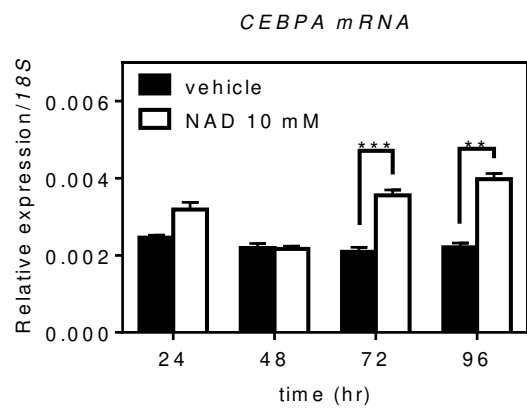
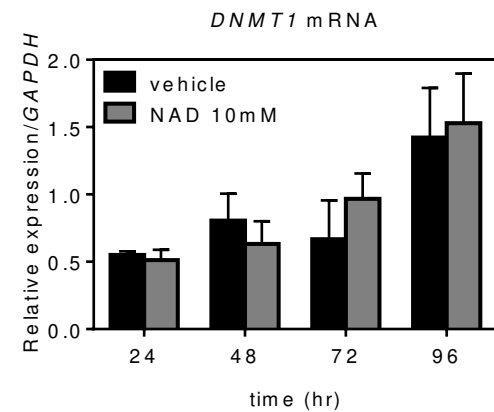
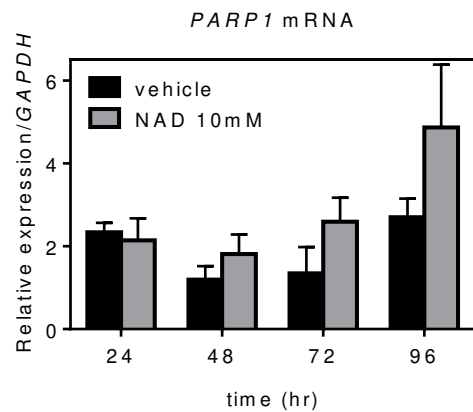
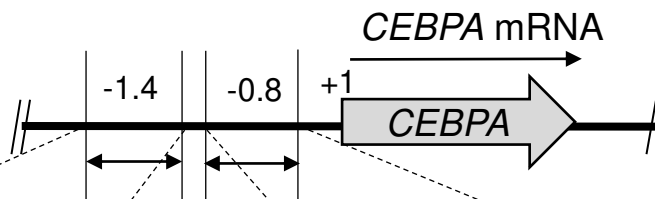
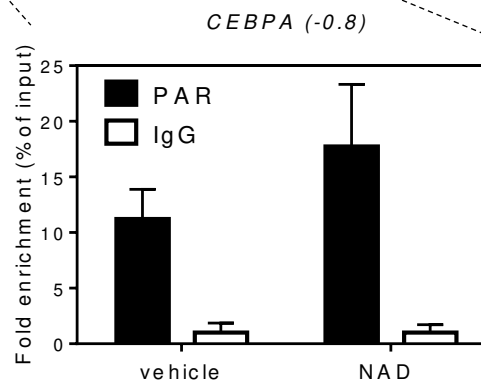
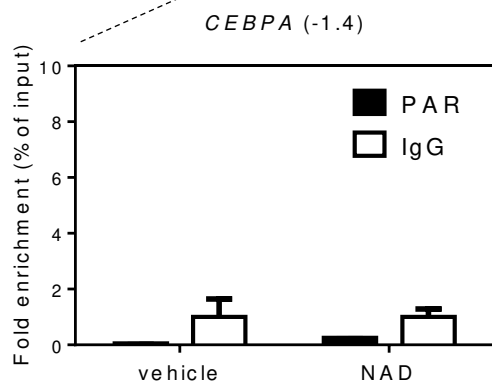
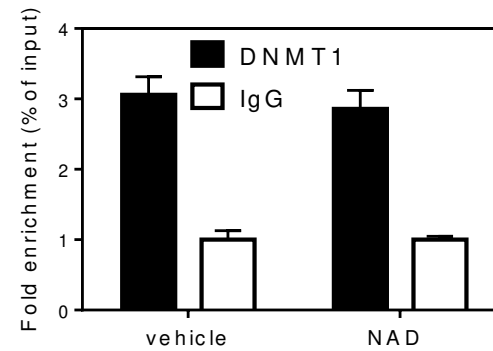
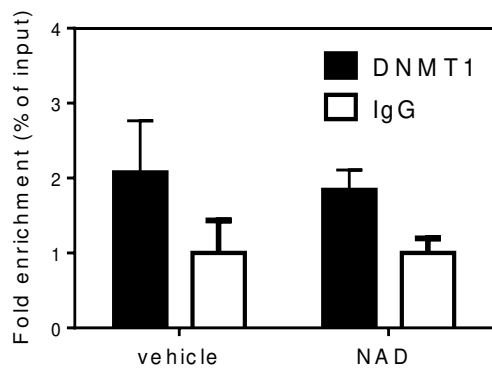
620

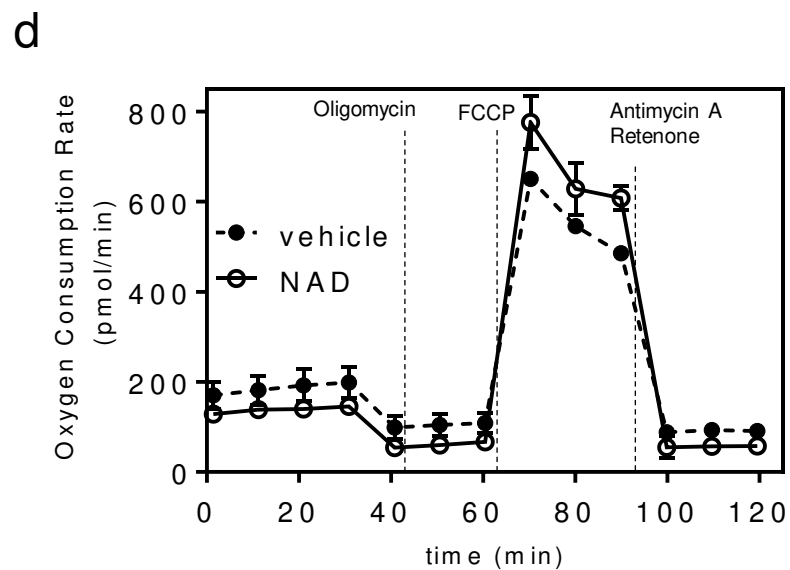
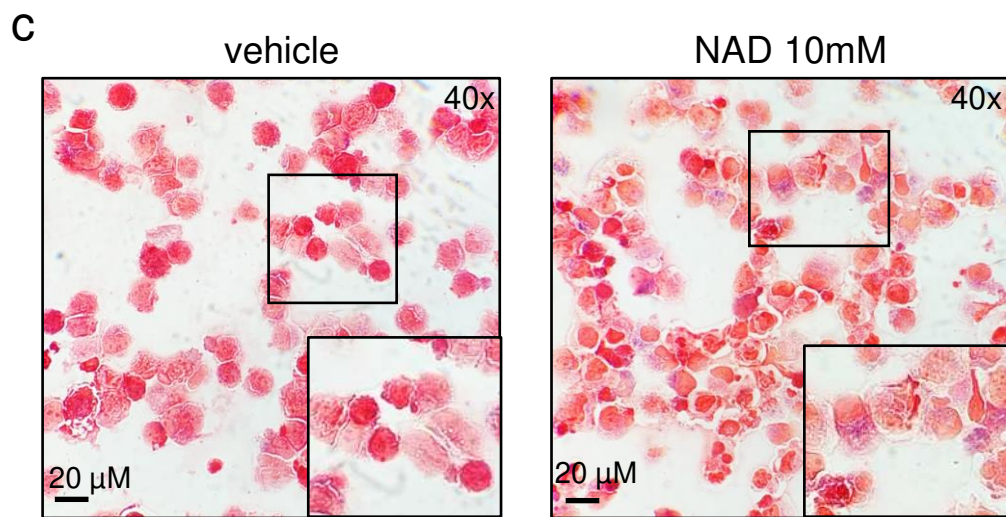
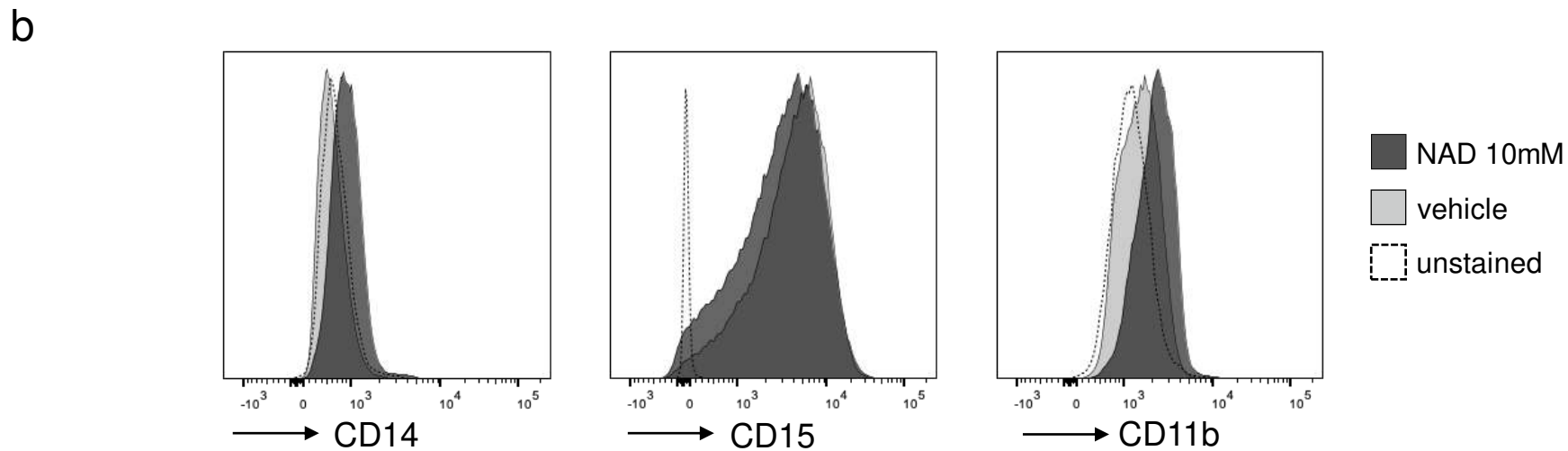
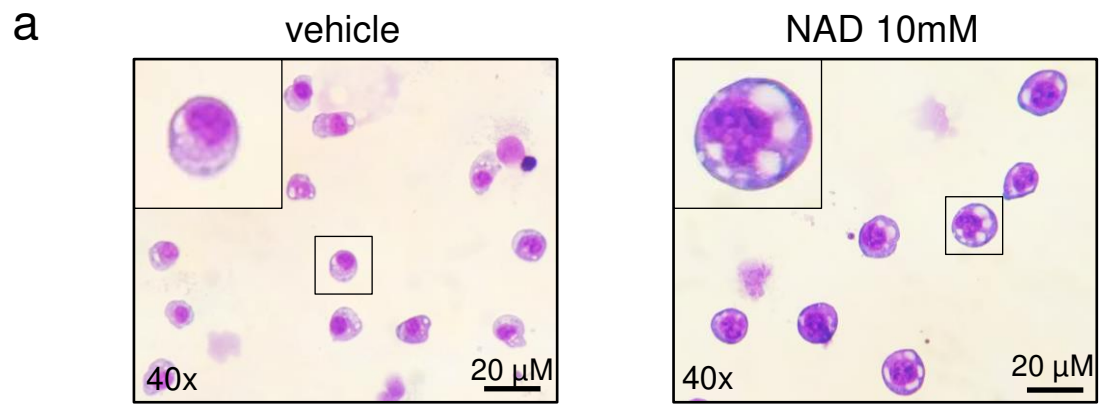
621



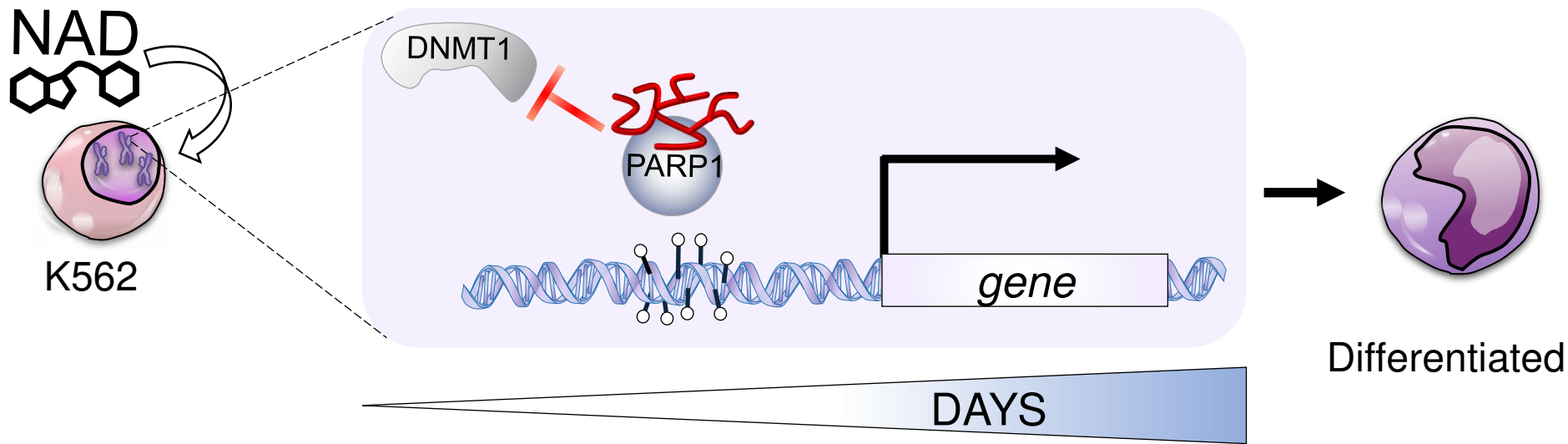
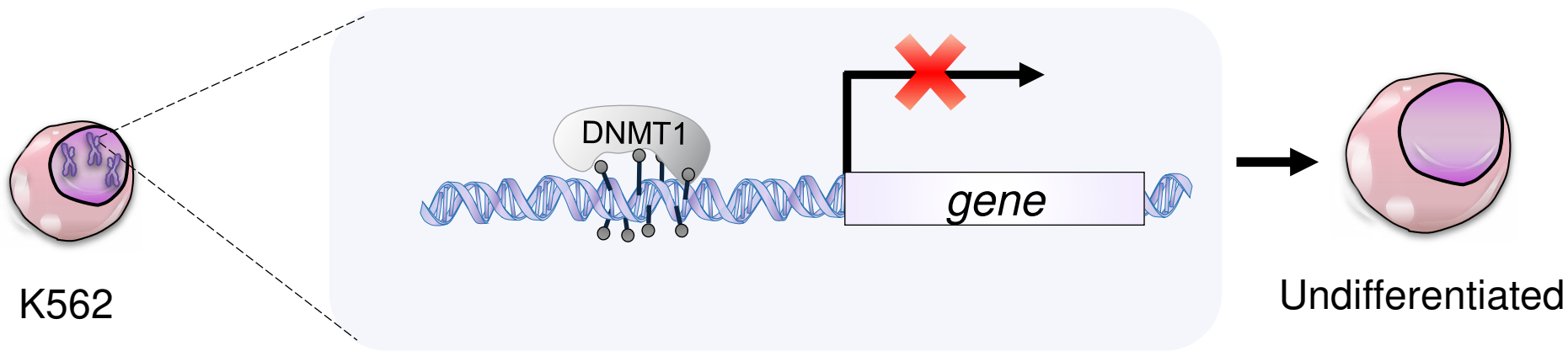




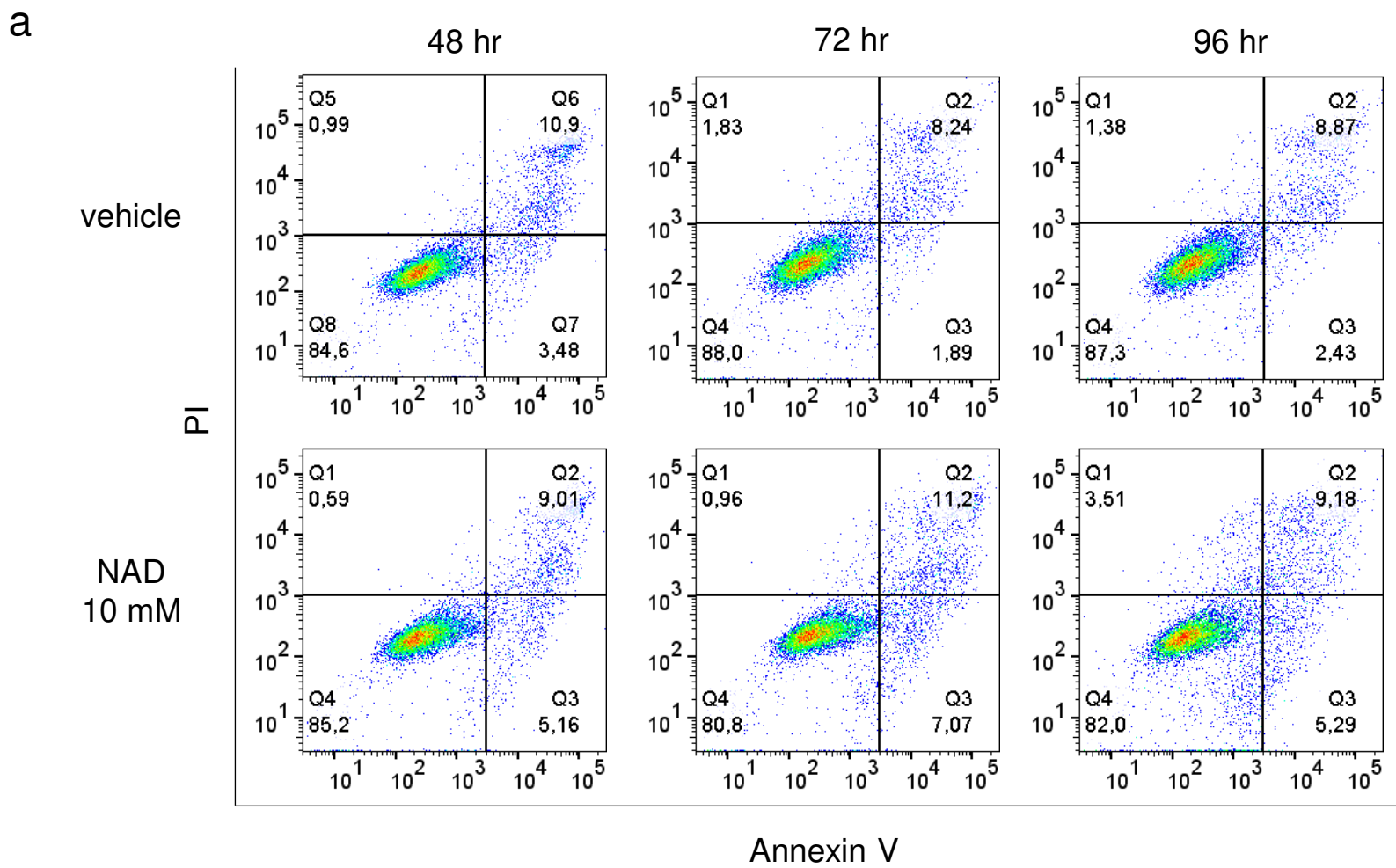
**a****b****c****d****e**



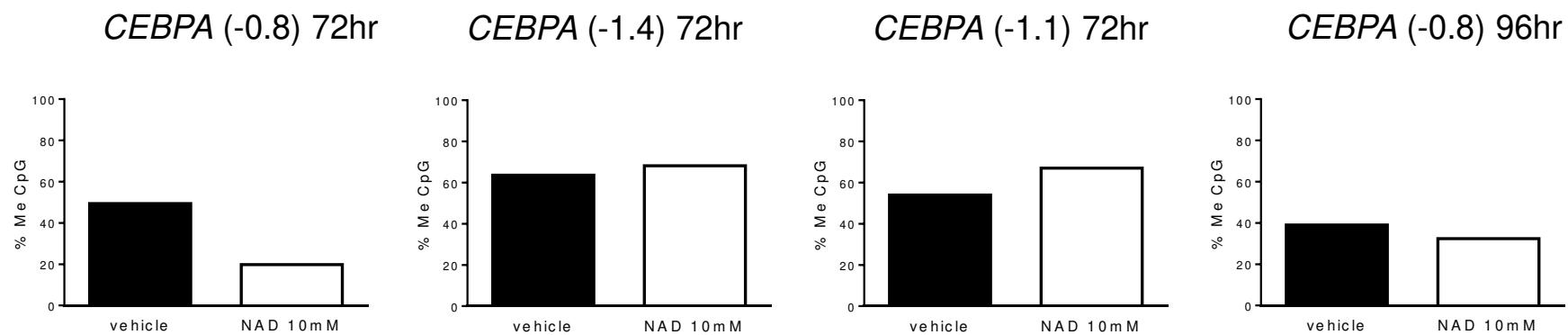
e



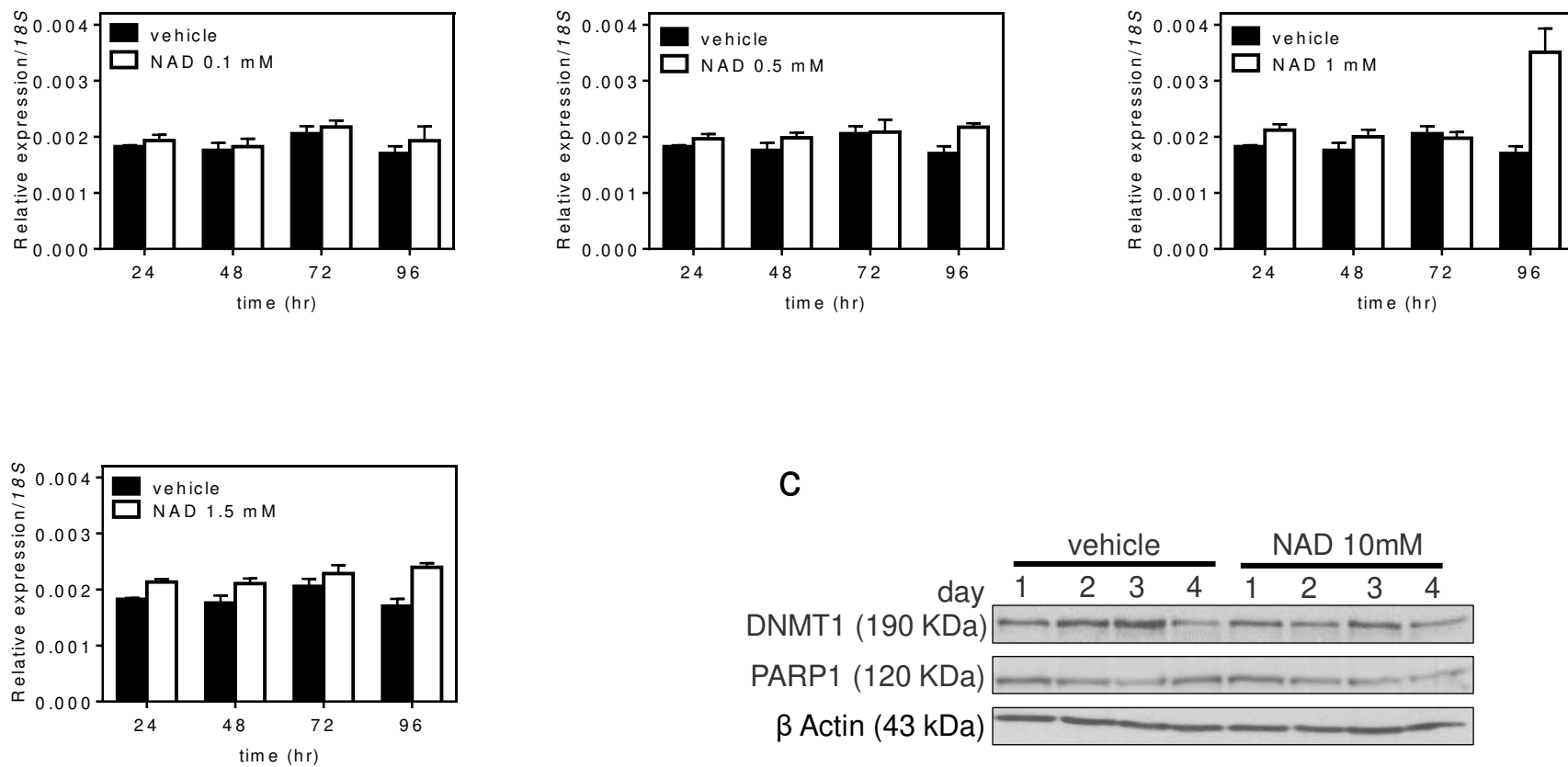
● Methylated cytosine; ○ Unmethylated cytosine



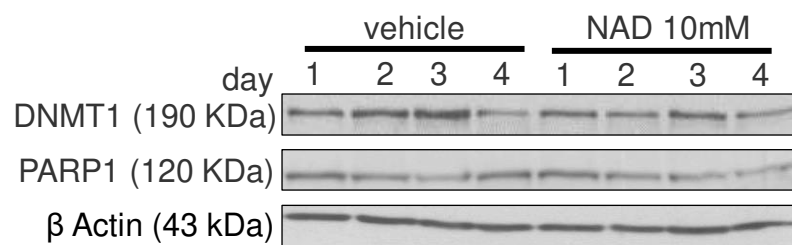
a



b



c



a

